

Design of a 5-cm Monopod Hopping Robot

Terence E. Wei, Gabriel M. Nelson, Roger D. Quinn, Hiten Verma, Steven L. Garverick
Case Western Reserve University
Cleveland, Ohio 44106

Abstract

The monopod hopper described here fits into a cube that is 5 cm on a side, is autonomous, and is designed to be statically and passively dynamically stable. Hopping is achieved through the excitation of a spring-mass system at its resonant frequency. Simulations were extensively used to finalize the design, before construction of the robot. The hopper, although having no active directional control, is able to climb steps up to 1mm, travel at a rate of 1.5 body lengths per second for an average of over 225 cm before deviating significantly from its original course, and can operate up to 45 min before depleting the energy stored in the batteries.

1. Introduction

Legged robots have been under development for decades. Having less of the limitations of wheeled or tracked vehicles, legged robots are more versatile, and are better suited for uneven or discontinuous terrain. In addition, the development of legged robots can aid in the understanding of human and animal locomotion (Raibert, 1986; Ritzmann et al, 1999).

Although the majority of the research done on legged robots has dealt with vehicles having multiple legs, a significant amount of research has been performed on single-legged robots. Raibert (1986; 1993) developed several monopod robots that hop. Although they were not statically stable, their controllers achieved active dynamic stabilization. He showed that the control theory that governs the performance of monopod robots could be used to control multi-legged ones. For instance, he linked two monopods together, and demonstrated that the two of them could operate together as a biped in a one foot gait (Raibert, 1986).

In contrast, Ringrose (1997) developed several monopod robots that are not only statically stable, but are also passively dynamically stable. The special shape of its foot creates this stability. The foot's curvature causes a restoring torque to be imparted to the robot if it begins to tip over (Ringrose, 1997). Kingsley (1999) also developed a monopod hopping robot based on this principle and his work formed the basis for the robot described here.

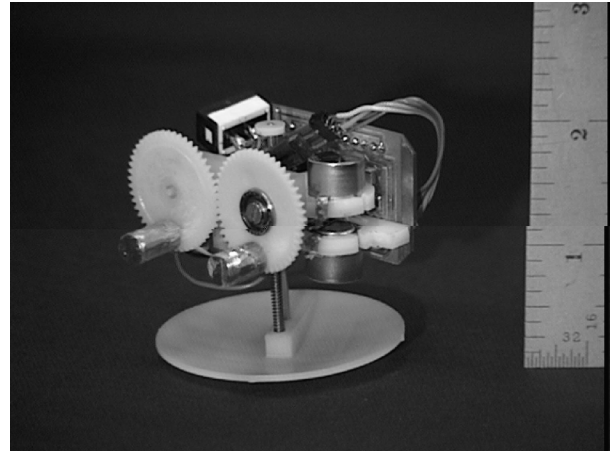


Figure 1. 5-cm Monopod Hopping Robot

This paper describes an autonomous monopod hopping robot that fits into a cube that is 5 cm on a side and is statically and passively dynamically stable.

2. Simulation and Design

2.1. Configuration of the robot

The original design for the hopper (see Figure 1) consisted of five major components. The first is the foot of the robot, which is designed with a constant radius of curvature, such that the bottom of the foot is spherical. As shown in Fig. 2, the center of curvature of the foot is located above the robot, and thus above the center of gravity, creating static stability. A foot with the proper radius of curvature causes just the right amount of restoring torque to be imparted to the robot if it begins to tip over. A radius of curvature that is too large will impart too much restoring torque to the robot upon impact with the ground, while a foot with a radius of curvature that is too small will not create enough restoring torque. Unless the foot is unusually wide, both cases will result in the hopper falling over. The foot is 5 cm in diameter and weighs 5g.

Attached to the foot of the robot are two shafts that the body of robot is free to slide upon. Both shafts are parallel to the vertical axis of the robot. One of the shafts extends up from the center of the foot. Two shafts

are used in order to prevent the body of the hopper from twisting as it travels up and down the shafts.

The body of the robot contains most of the vital components of the hopper including the Smoovy three-pole stepper motor that causes the actuation, the phase-lock loop (PLL) controller that drives the motor, and the batteries. Any two poles of the stepper motor can be active simultaneously, and the PLL controller measures the current in the inactive pole to determine the rotor's position. A miniaturized version of the PLL controller sold by Smoovy for use with its stepper motors. The total weight of the body is 30g.

A spring, coaxial with the shaft that is located at the center of the robot, connects the body to the foot. As the body of the robot travels up and down the shafts, energy is stored in the spring, creating a mass-spring system. The motor spins two disks, each with a mass offset from its center, at the damped natural frequency of the system to actuate the hopper. The axles of the disks are rigidly connected to the body of the robot. The disks are mounted such that as the eccentric masses spin, a periodic force is created only along the vertical axis of the robot. Due to counter-rotation, non-vertical forces created by one eccentric mass cancel out the non-vertical forces created by the other mass.

2.2. Simulation

Simulations were developed in order to choose the hopper's design parameters and predict its performance. It was not known how sensitive the system would be to changes in the weight of the different components or other variables, such as spring stiffness. In addition, it was not known how high the robot would be able to hop, what parameters would maximize hopping height or horizontal displacement, and what types of obstacles the robot would be able to climb or how it would recover from an impact with an obstacle.

In the simulation, the robot was restricted to move in a plane. The 2-D simulated robot had five degrees of freedom: the horizontal (x) and vertical (y) translations of the center of curvature of the foot, the distance from the center of mass of the body to the center of curvature of the foot (l), the rotation of the robot about the z axis with respect to vertical (θ), and the angular position of the eccentric masses (β).

The foot was simulated to be a collection of 14 points, instead of a continuous curved surface. Simulating the foot as a series of discrete points simplified the task of determining the forces from the environment and the

effects of the foot skidding across the ground (Nelson and Quinn, 1995). The horizontal and vertical forces on the n^{th} point of the foot are $F_{\text{foot},x}^n$ and $F_{\text{foot},y}^n$, respectively. Each point has a set of local coordinates that defines its position (p_x and p_y).

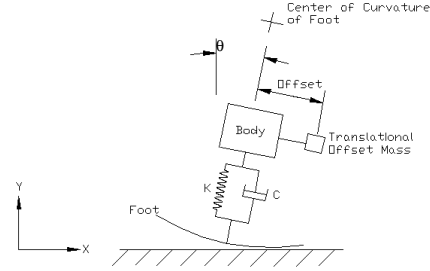


Figure 2. The simulated 2-D robot has five degrees of freedom. Environmental forces were modeled with springs and dampers.

A translational offset (balance) mass is also included in the equations of motion. This translational offset mass causes the robot to tip by a few degrees, causing locomotion in the direction that the robot is leaning towards, but not interfering with the robot's passive static and dynamic stability. The friction between the body of the robot and the shafts that it slides on is included in the F_{springs} terms. The horizontal and vertical forces from the ground are $F_{g,x}$ and $F_{g,y}$ respectively. ' denotes a derivative with respect to time.

The notation used in the following equations is as follows:

- d_1 = distance of the center of curvature of the foot to the center of mass of the foot
- d_2 = distance of translational offset mass from body
- m_1 = mass of the body
- m_2 = mass of the foot
- m_3 = mass of each eccentric mass
- m_4 = mass of the translational offset mass
- r_g = radius of gyration of eccentric masses
- r_c = radius of curvature of the foot
- G = gravitational acceleration

The first four equations of motion are as follows:

$$\begin{aligned}
 m_1 \cdot x'' + m_2 \cdot x'' - 2 \cdot m_2 \cdot \theta' \cdot l' \cdot \cos(\theta) - \\
 m_2 \cdot (d_1 - l) \cdot \theta' \cdot \theta' \cdot \sin(\theta) - m_2 \cdot l'' \cdot \sin(\theta) + \\
 m_2 \cdot d_1 \cdot \theta'' \cdot \cos(\theta) - m_2 \cdot l \cdot \theta'' \cdot \cos(\theta) = \\
 F_{g,x} - F_{\text{eccentric masses}} = \sin(\theta) + 2 \cdot m_2 \cdot l \cdot \theta' \cdot \cos(\theta) \\
 + m_2 \cdot (d_1 - l) \cdot \theta' \cdot \theta' \cdot \sin(\theta) + m_4 \cdot d_2 \cdot \theta' \cdot \theta' \cdot \cos(\theta) \quad (1)
 \end{aligned}$$

$$m_1 \cdot y'' + m_2 \cdot y'' + m_2 \cdot G + m_2 \cdot G - 2 \cdot m_2 \cdot l' \cdot \theta' \cdot \sin(\theta) +$$

$$\begin{aligned}
& m_2 \cdot (d_1 - l) \cdot \theta' \cdot \theta' \cdot \cos(\theta) + m_2 \cdot l'' \cdot \cos(\theta) + \\
& m_2 \cdot l'' \cdot \cos(\theta) + m_2 \cdot d_1 \cdot \theta'' \cdot \sin(\theta) - m_2 \cdot l \cdot \theta'' \cdot \sin(\theta) \\
& = F_{g,y} - F_{\text{eccentric masses}} \cdot \cos(\theta) - m_1 \cdot G - 2 \cdot m_3 \cdot G - \\
& m_2 \cdot G - m_4 \cdot G + 2 \cdot m_2 \cdot l' \cdot \theta' \cdot \sin(\theta) - \\
& m_2 \cdot (d_1 - l) \cdot \theta' \cdot \theta' \cdot \cos(\theta) + m_4 \cdot d_2 \cdot \theta' \cdot \theta' \cdot \sin(\theta) \quad (2)
\end{aligned}$$

$$\begin{aligned}
& m_2 \cdot G \cdot \cos(\theta) + m_2 \cdot (d_1 - l) \cdot \theta' \cdot \theta' + m_2 \cdot l'' - m_2 \cdot x'' \cdot \sin(\theta) \\
& + m_2 \cdot y'' \cdot \cos(\theta) = F_{\text{springs}} + F_{g,y} - F_{g,x} - \\
& m_2 \cdot G \cdot \cos(\theta) - m_2 \cdot (r_c - l) \cdot \theta' \cdot \theta' \quad (3)
\end{aligned}$$

$$\begin{aligned}
& m_2 \cdot G \cdot d_1 \cdot \sin(\theta) - 2 \cdot l' \cdot \theta' \cdot d_1 \cdot m_2 + I_{zz} \cdot \theta'' + m_2 \cdot l \cdot l \cdot \theta'' + \\
& m_2 \cdot d_1 \cdot x'' \cdot \cos(\theta) + m_2 \cdot d_1 \cdot y'' \cdot \sin(\theta) - \\
& m_2 \cdot G \cdot l \cdot \sin(\theta) + 2 \cdot m_2 \cdot l \cdot l' \cdot \theta' - 2 \cdot m_2 \cdot l \cdot d_1 \cdot \theta'' - \\
& m_2 \cdot l \cdot x'' \cdot \cos(\theta) - m_2 \cdot l \cdot y'' \cdot \sin(\theta) = \\
& - F_{g,x} \cdot l \cdot \cos(\theta) + \Sigma(F_{\text{foot},y}^n \cdot p_x) \cdot \cos(\theta) - \\
& \Sigma(F_{\text{foot},x}^n \cdot p_y) \cdot \cos(\theta) - l \cdot F_{g,y} \cdot \sin(\theta) - \\
& \Sigma(F_{\text{foot},x}^n \cdot p_x) \cdot \sin(\theta) - \Sigma(F_{\text{foot},y}^n \cdot p_y) \cdot \sin(\theta) - \\
& m_2 \cdot G \cdot d_1 \cdot \sin(\theta) + 2 \cdot l' \cdot \theta' \cdot d_1 \cdot m_2 + m_2 \cdot G \cdot l \cdot \sin(\theta) - \\
& 2 \cdot m_2 \cdot l \cdot l' \cdot \theta' - m_4 \cdot d_2 \cdot y' \cdot \theta' \cdot \sin(\theta) - m_4 \cdot d_2 \cdot G \cdot \cos(\theta) \quad (4)
\end{aligned}$$

These four equations are numerically integrated using the 4th order Runge Kutta method. The force caused by the counter rotating eccentric masses is described by

$$F_{\text{eccentric}} = 2 \cdot m_3 \cdot r_g \cdot \beta' \cdot \beta' \cdot \cos(\beta) + 2 \cdot m_3 \cdot \beta'' \cdot \sin(\beta) \quad (5)$$

The acceleration of the eccentric masses is calculated assuming that the motor is generating its maximum torque ($\tau_{\text{motor max}}$).

$$\begin{aligned}
(2 \cdot m_3 \cdot r_g \cdot r_g) \cdot \beta'' = \\
(\tau_{\text{motor max}} + 2 \cdot m_3 \cdot r_g \cdot G \cdot \sin(-\theta + \beta) + \\
2 \cdot m_3 \cdot r_g \cdot y'' \cdot \sin(-\theta + \beta)) \quad (6)
\end{aligned}$$

The resulting velocity is then compared to the desired angular velocity. If the resulting angular velocity is higher than the desired, then the velocity is set equal to the desired, and the acceleration is recalculated. A 5mm Smoovy stepper motor was selected to drive the actuation of the robot due to its small size and high power to weight ratio. The maximum torque that the motor can develop with a transmission ratio of 1:25 is only 2.85 mNm, resulting in frequent drops in angular velocity below the desired speed.

The simulation appeared to model well the hopper's performance on flat ground. Unfortunately, the modeling of the foot of the robot as a series of points prevented the simulation from climbing steps in a realistic manner. As the hopper attempted to climb up or down steps, the corner of the step would penetrate the surface of the foot between the points, creating unrealistic forces on the foot.

The relationship between the robot's stable hopping height and changes to masses or other properties of the hopper was determined (see Figure 3). The stable hopping height is the highest point that the bottom of the foot reaches when the hopping of the robot has reached steady state.

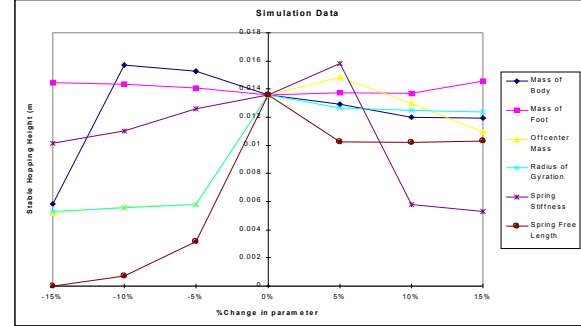


Figure 3. Sensitivity of the stable hopping height to changes in the design parameters.

This information is important because many properties modeled in the simulation, such as ground stiffness or the friction between the shafts and the body of the robot, were not known accurately or would require complex modeling that exceeds the scope of the project. Also, although there were many properties that could be changed by design, it was unknown how close the properties of the final, constructed robot could be made to the desired design. For instance, the manufacturer stated that the custom made springs could only be made within 10% of the desired stiffness. The simulation was able to aid in determining what effects these perturbations would make in the performance of the robot.

The data in Figure 3 indicates that an improvement could be made to the design by increasing the weight of the eccentric masses by 5%. Increases in the weight of the eccentric masses can increase the actuator force. However, large eccentric weights will prevent the motor from operating at an adequate speed, which is why the stable hopping height declines for increases larger than 5%.

The data also indicates that changes to the free length of the spring would have detrimental effects on the stable hopping height of the robot. If the free length is reduced, then the spring becomes fully compressed. The sharp change in stiffness that occurs to the spring when the spring reaches its solid length causes an abrupt deceleration in the body of the robot. The motion of the body then becomes slightly out of phase with the spinning eccentric masses, reducing the stable hopping

height. A stop is located on the top of the shafts, and it is designed to prevent the body of the robot from leaving the shafts. The data indicates that increases in the free length of the spring will cause the body of the robot to hit the stop. The effect is similar to what happens when the spring is fully compressed.

2.3. Design Parameters

The design parameters for the robot were chosen through use of the previously described simulation. The radius of curvature of the foot was determined by simulating the effects of 1) a fall from rest from a 10 cm height and a 10 degree rotation, and 2) a fall from a 10 cm height, no rotation, and a 1 m/s horizontal velocity. A radius of curvature of 6.7 cm allowed the robot to recover from both tests without tipping over.

The determination of the optimal weight of the eccentric masses was made difficult because of the limitations of the motor and the size of the hopper. The maximum motor torque limited their mass. The eccentricity of these masses was also limited by the goal of making the microrobot fit into a cube 5cm on a side. The restrictions of the motor forced the design to incorporate smaller masses that are excited at a higher frequency. In simulations, higher frequencies allowed the eccentric masses to create enough force to cause stable hopping heights of over 1cm. Hops of this height were achieved with the frequency of the spinning of the eccentric masses and the frequency of the hops equal and in phase. Simulation data indicated that even higher hops could be achieved if the driving frequency was double that of the hopping frequency. However, driving the eccentric masses at double the hopping frequency either required more torque or more speed than the motor could provide.

The simulation indicated that the eccentric masses should be 8.4g and have a radius of gyration of 0.89 cm. A spring with a stiffness of 115 N/m and a free length of 2.54 cm would cause the natural frequency of the system to be approximately 6.5 Hz, which was determined to be the desired frequency.

2.4. Power Source

The primary considerations for a power source for the robot were high energy density, small physical dimensions and the ability to supply the current and voltage required by the motor to operate satisfactorily. The class of Lithium batteries available commercially seemed suitable for the application. For a given weight, Lithium cells store the

highest energy and also have the highest maximum discharge current.

The motor would require at least 6 volts to run as desired. The average current drawn by the motor and controller was 120 mA, but was not constant due to the mechanics of the robot.

The experimental data collected using resistive loads on the DL1/3N showed that the battery could in fact supply a current of the order of 100 mA for over 15 minutes. Tests on the batteries with the actual motor were even more promising as the series combination of 3 DL1/3N cells could maintain a voltage of over 6V across the motor for 22 minutes.

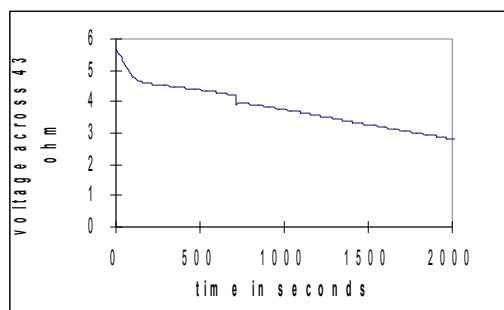


Figure 5. Voltage of 2 DL1/3Ns over a 43ohm resistor vs. time.

3. Results

Although the results from various tests were promising, the hopper was hindered by the inability of the PLL controller to drive the stepper motor at a low enough speed. Experimentally, it was determined that the PLL controller could only drive the motor at speeds higher than 9 Hz, when the desired was 6.5 Hz (see Figure 6).

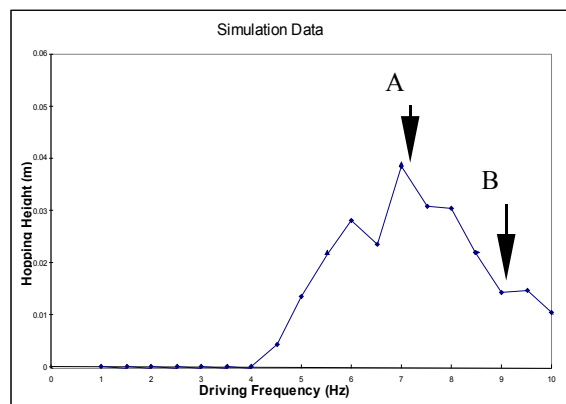


Figure 6. Driving Frequency vs. Stable Hopping Height from simulation. Point A indicates the optimal frequency. Point B indicates the lowest speed the PLL controller could provide.

At speeds slower than 9 Hz, the PLL controller is unable to determine the position of the rotor because the current created in the inactive pole is too small to be measured. This cut the potential hopping height of the microrobot by almost two-thirds according to the simulation. A change was made to the design to raise the resonance frequency above 9 Hz. Two compression springs were placed on the center shaft of the robot. These springs were placed such that one spring was compressed when the body of the robot traveled down the shafts. The other spring was compressed when the body of the robot traveled up the shafts. The motor was then operated at a speed of 9.2 Hz, which was the new damped natural frequency of the system.

The hopper was tested to determine its average horizontal velocity. The linear distance that the hopper was able to traverse in 3 sec was recorded. Over 10 trials, the average rate was 7.75 cm/sec, or 1.5 body lengths per second.

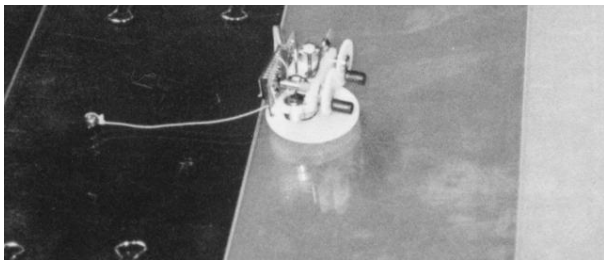


Figure 7. Hopper climbing a staircase. A tail was added to provide passive direction control.

A series of tests were performed on the 5cm monopod hopper at the DARPA Distributed Robotics Principal Investigators' Meeting, held in the Quantico US Marine Corps Base in September, 1999. A staircase was constructed with 4 steps (see Figure 7). Each step was 15 cm long by 30 cm wide. The height of each of the steps was adjustable so that the hopper could attempt staircases of varying heights. At step heights of 0.5 mm, the climbing of the steps was fairly consistent. Out of a total of 20 trails, the hopper was able to climb the first step 16 times (see Figure 8). The hopper has no means to turn itself, or detect when it is no longer pointed in the desired direction. Even though a tail was added to the robot to provide passive direction control (Fig. 7), the hopper often turned until it was no longer facing up the staircase.

	Staircase with 0.5mm steps	Staircase with 0.75mm steps	Staircase with 1mm steps
Total Number of Trials	20	10	10
Number of times the first step was climbed	16	8	2
Number of times the second step was climbed	11	4	0
Number of times the third step was climbed	7	1	0
Number of times the fourth step was climbed	4	0	0

Figure 8. Results from tests of the hopper attempting to climb staircases of varying heights.

Next, the staircase was adjusted such that the step height was 0.75 mm. The hopper climbed the first step 8 out of 10 times. However, its success at the successive steps was lower than the trials at a step height of 0.5 mm.

The staircase was then adjusted such that the step height was 1mm. Out of a total of ten trials, the hopper was only able to climb the first step twice.

The hopper was then subjected to a Range of Locomotion test (see Figure 9). The hopper was placed into a hallway 1m wide, with walls on both sides. The hopper was then set free, and the furthest distance the hopper was able to go down the hallway was recorded. There were three possible modes of failure in this test. The hopper could have had a mechanical or power failure. The robot could have also had a positional failure, which would have occurred in the event that the robot turned to face a wall or turned completely around to travel towards the starting point. If the robot turned to face a wall, the test was continued until it was clear that the robot could not turn back and continue to make forward progress. The condition in which the robot fell onto its side would have also been classified as a positional failure. However, this did not occur during any of the trials of the Range of Locomotion test.

	Distance Traveled (cm)	End Condition
Trial 1	274	Positional
Trial 2	338	Positional
Trial 3	46	Positional/Reversal
Trial 4	137	Positional/Reversal
Trial 5	145	Positional/Reversal
Trial 6	312	Positional
Trial 7	330	Positional
Trial 8	300	Positional
Trial 9	264	Positional
Trial 10	104	Positional/Reversal

Figure 9. Results from Range of Locomotion tests.

This Range of Locomotion test was performed 10 times. The average distance the hopper was able to move without failure was 225 cm. All ten trials were terminated due to positional failures. There were no mechanical or power failures and the robot never tipped over during these tests. The end condition "positional/reversal" in Table 2 indicates the tests in which the robot completely turned around and attempted to return to the starting location. The robot caused all other positional failures by turning such that forward progress could no longer be achieved.

Finally, a test was performed to determine how long the robot could operate before depleting the energy stored in the batteries. Fresh batteries were placed in the hopper, and it ran continuously for 45 minutes before operation ceased. The current draw was measured during operation of the robot, and the motor and controller together drew an average of 120 mA.

4. Conclusions

An autonomous hopping robot was constructed that could fit into a 5 cm cube. The success of the robot was proved by its ability to consistently travel more than 225 cm in one direction without tipping over. Furthermore, the ability of the robot to function for 45 minutes without tipping over demonstrates its low power consumption.

The results of the tests performed on the hopper indicated that the performance would be significantly improved if the hopper could be controlled to point in the desired direction. All of the failures during the range of locomotion tests were due to the robot turning to face a wall or to point back towards the starting location. If the robot could be kept pointed in the same direction for the duration of the range of locomotion test, the robot could potentially travel down the test track until the batteries are depleted, which would be significantly longer than the 225 cm average currently attainable. In addition, a higher percentage of the

staircases could have been climbed had the robot been pointed in the correct direction for the duration of the test. Although a tail helped to prevent the robot from turning, it is clear that the robot will eventually turn unless direction control comes from an active mechanism. The position of the translational offset mass could be changed in order to provide active directional control. Active directional control would be needed if the hopper was placed on a sloped surface. Without an active steering mechanism, the hopper will always turn to face down the slope.

Simulation data also indicates that much higher steps could be attempted if the system could be driven at a lower frequency. A more capable PLL controller would have resulted in much more impressive test results.

Significant energy loss resulted from the inefficiency of the transmission of the stepper motor and friction between the body of the robot and the shafts. A slight imbalance of the eccentric masses causes the robot to rock side to side as it is moving forward. Therefore, some energy is wasted in this rocking motion that could have been used to make the robot hop higher. Reduction of energy loss could have allowed the robot to hop higher and consume less power.

When the simulation is modified to reflect the unexpectedly high shaft friction and the increase spring stiffness that was intentionally introduced due to problems with the PLL controller, the simulation indicates that the hopper should achieve a maximum hopping height of 3 mm. However, because the simulation restricts the motion of the robot to a plane, the rocking motion that is observable while the robot is moving forward is not a motion that could be simulated.

Acknowledgements

This work was supported by the DARPA Distributed Robotics Program under contract DARPA/ETO DAAN02-98-C-4027. We would like to thank Matthew Birch for lending design and machining expertise, Yuandao Zhang for miniaturizing the PLL controller, and Jeff in the CWRU foundry for help with the melting and molding of the eccentric weights.

References

- [1] Kingsley, Dan. "Passively Stabilized Monopodic Hopping". 50th International Astronautical Congress, Amsterdam, The Netherlands, October 1999.
- [2] Nelson, G.M., and Quinn, R.D., "A Lagrangian

Quasicoordinate Formulation for Dynamic Simulations of Multibody Systems," pp.823-830, Vol.57-2, Proceedings of the ASME Dynamic System and Control Division, San Francisco, California, 1995.

- [3] Raibert, Marc H. "Legged Robots." *Biological Neural Networks in Invertebrate Neuroethology and Robotics*. Academic Press, Inc: New York. 1993.
- [4] Raibert, Marc H. *Legged Robots That Balance*. MIT Press: Cambridge, Massachusetts. 1986.
- [5] Ringrose, R. *Self-Stabilizing Running*. PhD Thesis, Department of Electrical Engineering and Computer Science, Massachusetts Institute of Technology, Cambridge, Massachusetts, 1996.
- [6] Ringrose, Robert. "Self Stabilizing Running". Proceedings of the 1997 IEEE International Conference on Robotics and Automation, Albuquerque, NM, 1997.
- [7] Ritzmann, R.E., R.D. Quinn, J.T. Watson, S.N. Zill. "Insect walking and biorobotics: A relationship with mutual benefits". *Bioscience* (in press). 1999.
- [8] Smoovy, <http://www.smoovy.com/>
- [9] Wei, Terence. *A 5cm Single-Legged Hopping*. MS Thesis, Department of Mechanical and Aerospace Engineering, Case Western Reserve University.